Experimental and analytical study on shear behavior of strain-hardening cementitious composite beams reinforced with fiber-reinforced polymer bars

Gu, Dawei; Pan, Jinlong; Luković, Mladena; He, Jixuan

DOI
10.1002/suco.202100544

Publication date
2022

Document Version
Final published version

Published in
Structural Concrete

Citation (APA)
Gu, D., Pan, J., Luković, M., & He, J. (2022). Experimental and analytical study on shear behavior of strain-hardening cementitious composite beams reinforced with fiber-reinforced polymer bars. *Structural Concrete*, *23*(2), 1080-1099. https://doi.org/10.1002/suco.202100544

Experimental and analytical study on shear behavior of strain-hardening cementitious composite beams reinforced with fiber-reinforced polymer bars

Gu, Dawei; Pan, Jinlong; Luković, Mladena; He, Jixuan

DOI
10.1002/suco.202100544

Publication date
2022

Document Version
Final published version

Published in
Structural Concrete

Citation (APA)
Gu, D., Pan, J., Luković, M., & He, J. (2022). Experimental and analytical study on shear behavior of strain-hardening cementitious composite beams reinforced with fiber-reinforced polymer bars. *Structural Concrete*, *23*(2), 1080-1099. https://doi.org/10.1002/suco.202100544

Received: 12 August 2021 | Revised: 7 October 2021 | Accepted: 27 November 2021

DOI: 10.1002/suco.202100544

ARTICLE

fib CEB-FIP WILEY

Experimental and analytical study on shear behavior of strain-hardening cementitious composite beams reinforced with fiber-reinforced polymer bars

Dawei Gu[1,2] | **Jinlong Pan**[1] | **Mladena Luković**[2] | **Jixuan He**[1]

[1]School of Civil Engineering, Southeast University, Nanjing, China

[2]Faculty of Civil Engineering and Geosciences, Delft University of Technology, Delft, The Netherlands

Correspondence
Jinlong Pan, School of Civil Engineering, Southeast University, Nanjing, China.
Email: cejlpan@seu.edu.cn

Funding information
National Natural Science Foundation of China, Grant/Award Number: 51778131

Abstract

Application of fiber-reinforced polymer (FRP) reinforcement in concrete beams may cause large deflection and crack width, as well as low shear capacity and ductility due to relatively small stiffness of FRP materials. To avoid these unfavorable factors and evaluate the shear behavior of FRP-reinforced structural members, a high-performance strain-hardening cementitious composite (SHCC) is introduced to substitute conventional concrete in reinforced beams, and four-point bending test is conducted in this study. Six FRP-reinforced SHCC beams with different transverse reinforcement ratios and shear spans, as well as one concrete reference beam, were tested. According to the test results, the FRP-reinforced SHCC beam showed enhanced shear carrying capacity and superior ductility compared with the concrete beams. The shear span to effective depth ratio as well as the stirrup ratio has a great influence on the shear behavior of FRP-reinforced SHCC beams, including the failure mode, load-carrying capacity, crack propagation, and ductility. Finally, a simplified truss-strut model for predicting shear carrying capacity of steel or FRP-reinforced SHCC beams is proposed, and a good agreement is achieved with the experimental results.

KEYWORDS

ductility, failure mode, fiber-reinforced polymer (FRP) reinforcement, shear strength, simplified truss-strut model, strain-hardening cementitious composite (SHCC)

1 | INTRODUCTION

To improve the durability of reinforced concrete (RC) structures, the use of fiber-reinforced polymer (FRP) reinforcement appears to be very promising since they assure a much higher corrosion resistance with respect to steel reinforcement.[1,2] However, due to the lower elastic modulus of FRP bars compared with that of steel, for the same reinforcement ratio, FRP-RC member will exhibit larger deflection and deeper cracks followed by larger crack widths. Thus, the design of FRP-RC members is usually governed by its serviceability limit state, with an insufficient utilization of the material's strength.[3,4]

The lack of ductility is another inherent drawback of FRP materials since they often fail due to brittle rupture without inelastic deformation. To avoid the brittle rupture of FRP bars in FRP-RC members, the over-reinforcing concept has been well adopted, which ensures that compressive failure of concrete takes place prior to the tensile rupture of FRP.[5,6] That means, the ductility of FRP-RC

Discussion on this paper must be submitted within two months of the print publication. The discussion will then be published in print, along with the authors' closure, if any, approximately nine months after the print publication.

members relies on the nonlinear deformation of concrete in compression zone. However, since concrete can exhibit very limited deformation capacity under compression due to its quasi-brittle behavior, poor ductility is always inevitable in FRP over-RC beams.

Poor shear carrying capacity is another problem for FRP-RC members. Compared with steel bars, the low modulus of elasticity of FRP reinforcement always leads to deeper and wider cracks in RC members under shear, which reduces the shear contribution from uncracked concrete and aggregate interlock. In addition, the dowel action is also weakened due to the limited transverse stiffness of FRP bars. Finally, the overall shear capacity of FRP-RC members would be lower than that of steel-RC members, and dense stirrups are always required in their shear design.[7,8]

To overcome the aforementioned drawbacks of FRP-RC members, replacing brittle concrete with strain-hardening cementitious composites (SHCC) would be a promising alternative.[9,10] Different from normal concrete and other types of fiber-RC, SHCC materials can exhibit a strain-hardening and multiple cracking response under uniaxial tension, with a remarkably high tensile strain capacity of 2% to 5% (200–500 times than that of concrete) and typical crack width ranging from 60 to 100 μm prior to peak strength.[11,12] When reinforcing SHCC with FRP bars, a compatible deformation can be achieved by preventing bond splitting and cover spalling with a reduced interfacial bond stress and relative slip.[9,13,14] However, the outstanding deformational capacity of SHCC can change the brittle failure of FRP-RC members into a ductile one, along with a significantly enhanced energy absorption behavior.[9,10,13,15,16]

Although there has been considerable research on the flexural response of FRP-reinforced SHCC members, investigations regarding their shear behavior are rare. Since the shear behavior of reinforced structural member is greatly influenced by the tensile properties of matrix, FRP-reinforced SHCC would exhibit quite different shear resisting mechanisms from that of concrete.[17–30] To investigate the shear behavior of FRP-reinforced SHCC beams, a set of four-point bending tests was conducted. The influence of different parameters (including matrix type, shear span, and transverse reinforcement ratio) on the load-carrying capacity, deformation ability, and ductility are evaluated. Finally, the prediction method of shear strength for both steel-reinforced SHCC beam and FRP-reinforced SHCC beam is proposed separately based on the truss and strut model.

2 | EXPERIMENTAL PROGRAM

2.1 | Material properties

The matrix of SHCC consisted of Ordinary Portland Cement (P.O 42.5), fly ash, silica fume, fine sand with a size ranged between 0.075 and 0.15 mm, water, cellulose, and superplasticizer, as shown in Table 1. The polyvinyl alcohol (PVA) short fiber with a diameter d of 39 μm, length l of 12 mm, tensile strength f_t of 1620 MPa, and tensile elastic modulus E of 42.8 GPa is used with a fraction of 2% in volume. The tensile stress–strain response of SHCC was determined using panel specimen with size of 150 mm × 150 mm × 40 mm, as shown in Figure 1. According to the uniaxial tension tests, a remarkable strain hardening response is achieved with ultimate tensile strain approaching 3% at mean peak tensile strength of 3.1 MPa, as shown in Figure 2. Commercial concrete was used for the reference beam. Three SHCC and concrete cubes (150 mm × 150 mm × 150 mm) were prepared from the same batch of beam fabrication and cured under the same condition as beam specimens. The average compressive strength of SHCC and concrete were tested to be 25.05 and 23.35 MPa, respectively, at the testing day of beam specimens (41 days), following Chinese National Standards GB/T 50107-2010.[31] The basalt FRP (BFRP) bars with diameters of 18 mm were used as tensile reinforcement, which have an ultimate tensile strength of 980 MPa and an elastic modulus of 40.5 GPa according to the manufacturer. The deformed steel bars with diameters of 20 and 8 mm were used as compressive reinforcement and stirrups, respectively, with the yield strength of 470 and 463 MPa. The steel rebars were used for stirrups since stirrups made of FRP can exhibit significant reduction in tensile strength due to the anisotropic characteristics and kinking action of bending fibers, which always leads to a premature failure near their bending corners.[32–34]

2.2 | Specimen preparation

A total of seven beams were fabricated, including six BFRP-SHCC beams and one BFRP-concrete counterpart beam. The over-reinforcing concept was adopted for the design of BFRP-reinforced beams, which means superfluous BFRP reinforcement in tension zone was provided to avoid the brittle rupture of BFRP bars.[35,36] The size of cross section was kept constant for all tested beams, with 210 mm in width and 300 mm in depth. All beams had a 150 mm overhang length beyond the supports on each side to enhance the anchorage of rebars. Three different lengths of 1700, 1900, and 2100 mm were designed to investigate effects of different shear span-effective depth ratios a/d, ranging from 2.07 to 2.82. Four types of transverse reinforcement ratio were designed, including 0%, 0.24%, 0.32%, and 0.48%. The details of all specimens are summarized in Table 2. Each specimen was identified by a couple of letters and a number. The prepositive letters "BRS" and "BRC" represent the BFRP-reinforced SHCC

TABLE 1 Mix proportion of SHCC (kg/m^3)

Cement	Fly ash	Silica fume	Sand	Water	Cellulose	Superplasticizer	Fiber
221.9	832.1	55.5	554.8	310.7	0.8	3.5	21.5

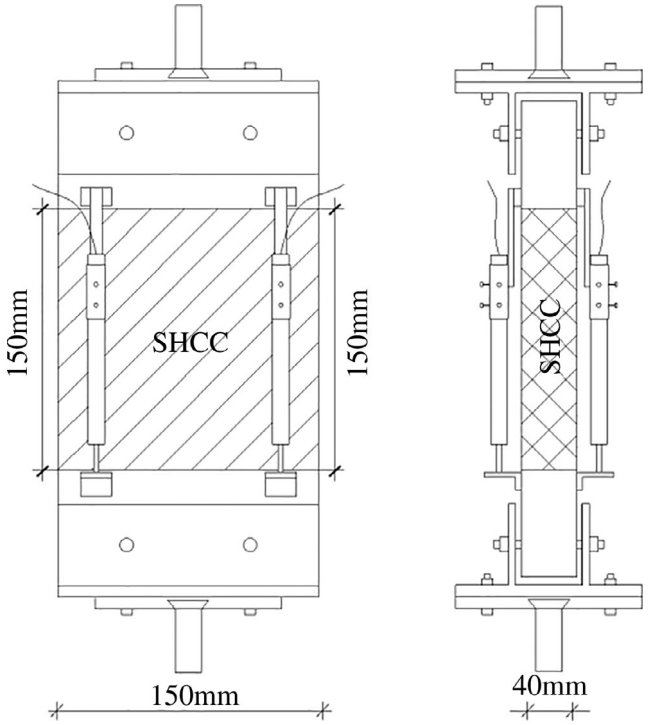

FIGURE 1 Uniaxial tensile tests of SHCC. SHCC, strain-hardening cementitious composite

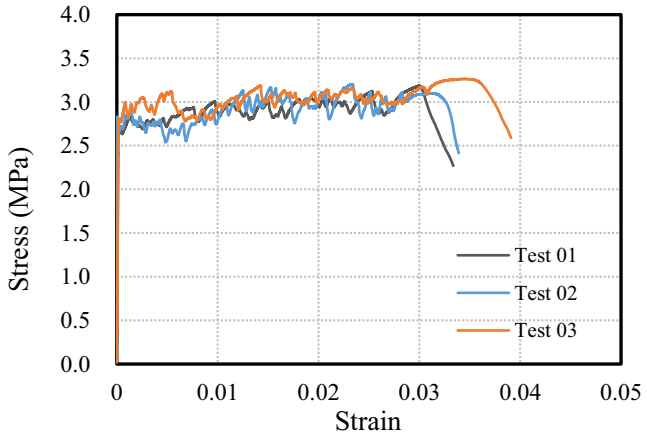

FIGURE 2 Tensile stress-strain relationship of SHCC. SHCC, strain-hardening cementitious composite

beam and BFRP-RC beam, respectively. The subsequent numbers "100," "150," or "200" indicate the stirrup spacing, and the beam without stirrups was represented by "NS." All these beams had a shear span of 650 mm. For specimens with extended shear span (750 mm) or shortened ones (550 mm), the characteristic letters "L" and "S" were added respectively. For example, "BRS-L200" represents a BFRP-reinforced SHCC beam with an extended shear span of 750 mm and stirrup spacing of 200 mm. Unlike other beams, specimen BRS-100 was reinforced with reduced longitudinal bars, which was designed to exhibit a flexural failure instead of shear for comparison.

2.3 | Test setup

Since BFRP bars are type of brittle reinforcement, conventional three-point bending test with a concentrated load may cause stress concentration at the middle span of beams, which can lead to the premature rupture of longitudinal BFRP reinforcement. Thus, all beams were tested under four-point bending, as shown in Figure 3. The test was controlled by displacement through the electronic universal testing machine with the capacity of 1000 kN, and load was monotonically applied at a stroke-controlled rate of 0.6 mm/minute until the ultimate failure (decreasing to 80% of peak load). One linear variable differential transformer was employed to monitor the mid-span deflection of the beam. All stirrups in shear span were instrumented with strain gauges. The applied load, displacements, and strain readings were synchronously recorded during the test, using a data acquisition system.

3 | EXPERIMENTAL RESULTS AND DISCUSSION

3.1 | Load–deflection behaviors and failure modes

3.1.1 | Specimens with different matrices

The load–deflection curves for beams and failure modes of different matrices are shown in Figure 4a. No matter for the concrete or SHCC specimen, the shear compression failure took place, which meant the ultimate shear strength was reached due to the crushing of

TABLE 2 Summary of tested specimens

Specimen	Matrix	Shear span (mm)	a/d	Main Bar Compression	Main Bar Tension	Stirrup	ρ_w(%)
BRC-150	Concrete	650	2.44	4C20	4C18	C8@150	0.32
BRS-NS	SHCC	650	2.44	4C20	4C18	—	0.00
BRS-200	SHCC	650	2.44	4C20	4C18	C8@200	0.24
BRS-150	SHCC	650	2.44	4C20	4C18	C8@150	0.32
BRS-100	SHCC	650	2.44	2C20	2C18	C8@100	0.48
BRS-S200	SHCC	550	2.82	4C20	4C18	C8@200	0.24
BRS-L200	SHCC	750	2.07	4C20	4C18	C8@200	0.24

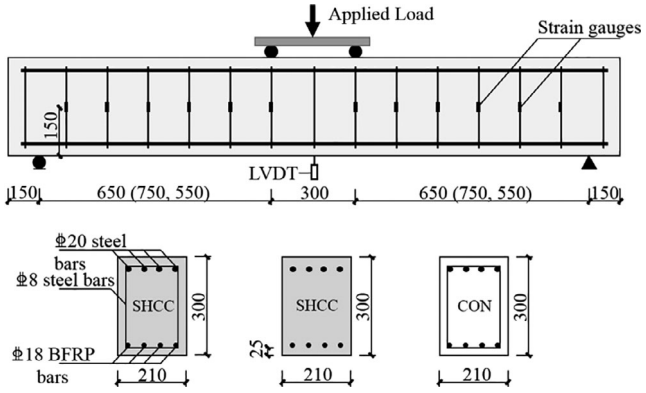

FIGURE 3 Test setup and specimen details (mm)

matrix in compression zone. Although the SHCC material has lower elastic modulus than concrete due to the absence of coarse aggregate, when reinforced with the same configuration of reinforcement, both of them exhibited similar stiffness before the peak load. In the concrete beam BRC-150, the first shear crack generated from the mid-height of beam section and then extended to both loading and supporting plates at an inclination of about 45°. Some splitting cracks were also observed along the longitudinal BFRP bars when the shear crack reached to the bottom of beam. Different from several major inclined shear cracks in concrete, a large number of multiple fine cracks were observed in SHCC before the localization of critical shear crack. After the ultimate shear strength was reached, the applied load showed a slight drop and then a ductile deformation plateau was achieved. Despite the absence of coarse aggregate interlock across cracks, such a ductile deformation plateau could be obtained through the friction between rough cracking surfaces, fiber bridging across cracks as well as the contribution from larger ultimate compressive strain of SHCC in shear compression zone. Finally, the shear-carrying capacity and deflection at the ultimate failure (defined once the load dropped to 80% of peak load) were increased by about 10% and 42%, respectively, when substituting concrete with SHCC for BFRP-reinforced beams. Besides this, the beam fabricated with SHCC exhibited a saturated cracking pattern between the support and loading point, as shown in Figures 4a and 5a, indicating a much better energy dissipation capacity than specimen made of conventional concrete in shear failure mode.

3.1.2 | Specimens with different transverse reinforcement ratios

The load–deflection curves for specimens of different shear reinforcement ratios are shown in Figure 4(b). It should be noted that the specimen BRS-100 with highest stirrup ratio was reinforced with only half the longitudinal bars of others, which was initially designed to exhibit a flexure failure instead of shear. Therefore, the stiffness of BRS-100 was obviously reduced when comparing with other specimens. For other three beams reinforced with the same amount of longitudinal BFRP reinforcement, their initial stiffness was not influenced by different stirrup ratios. However, when external load exceeded around 100 kN, the beam BRS-200 exhibited evidently higher stiffness than other counterpart specimens due to its postponed localization of critical shear crack, revealing a synergistic effect between the transverse reinforcement and SHCC matrix at a stirrup ratio of 0.24%. For the beam BRS-100 with highest stirrup ratio but reduced longitudinal BFRP reinforcement, more flexural cracks were observed and the diagonal shear cracks tended to open and propagate more quickly, resulting in an early localization of cracks in the shear span. At the peak load, the critical shear

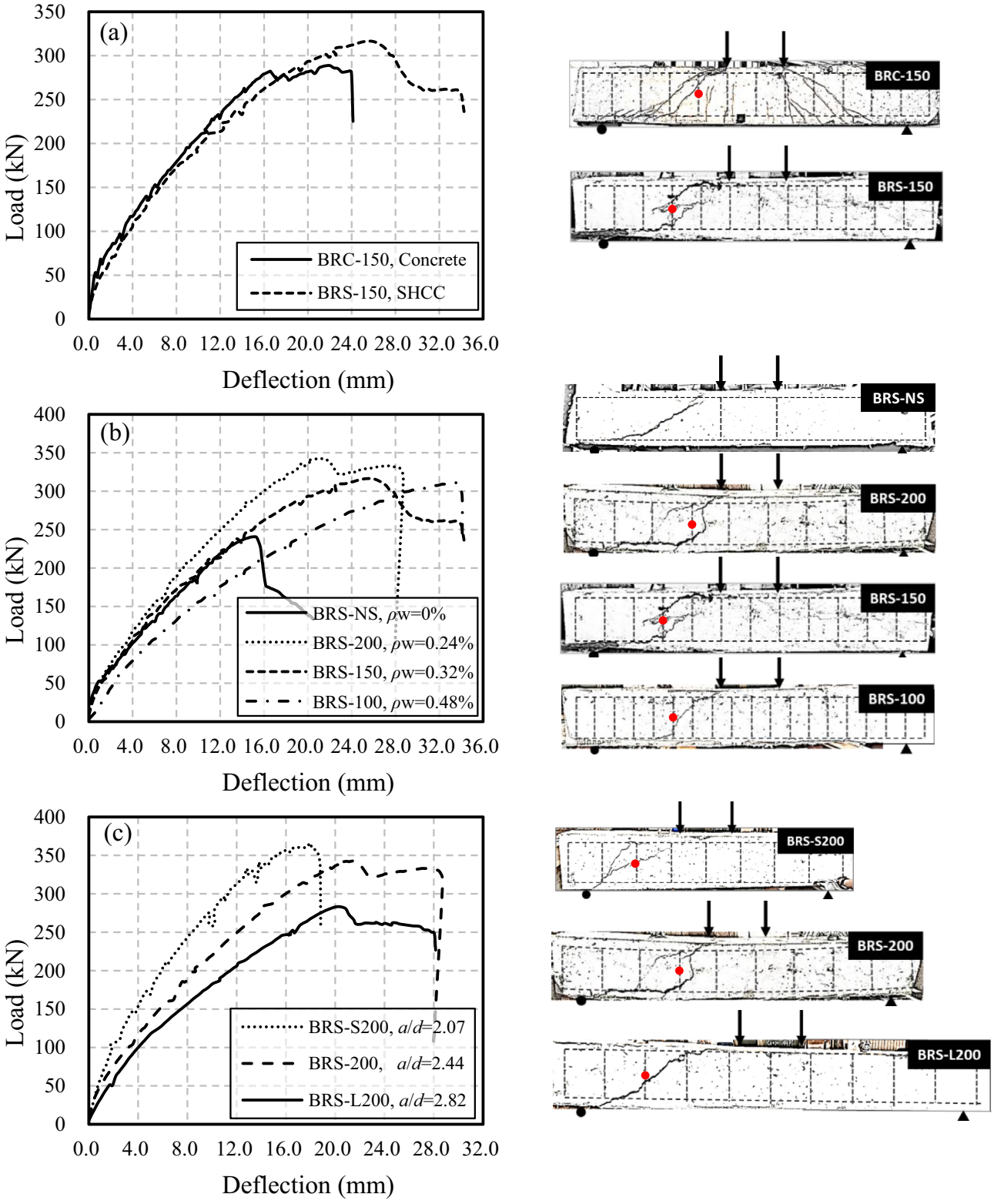

FIGURE 4 Load-deflection curves of tested beams and failure modes: (a) with different matrices; (b) with different transverse reinforcement ratios; (c) with different shear span to depth ratios (dashed lines represent the reinforcement configuration, and red points represent the selected gauges for later strain analysis)

crack had gone through the whole height of the shear span. It resulted in quite small-uncracked compressive zone for sustaining further deformation, and then the ultimate shear failure occurred immediately in a quite brittle manner although flexure failure was originally designed to happen.

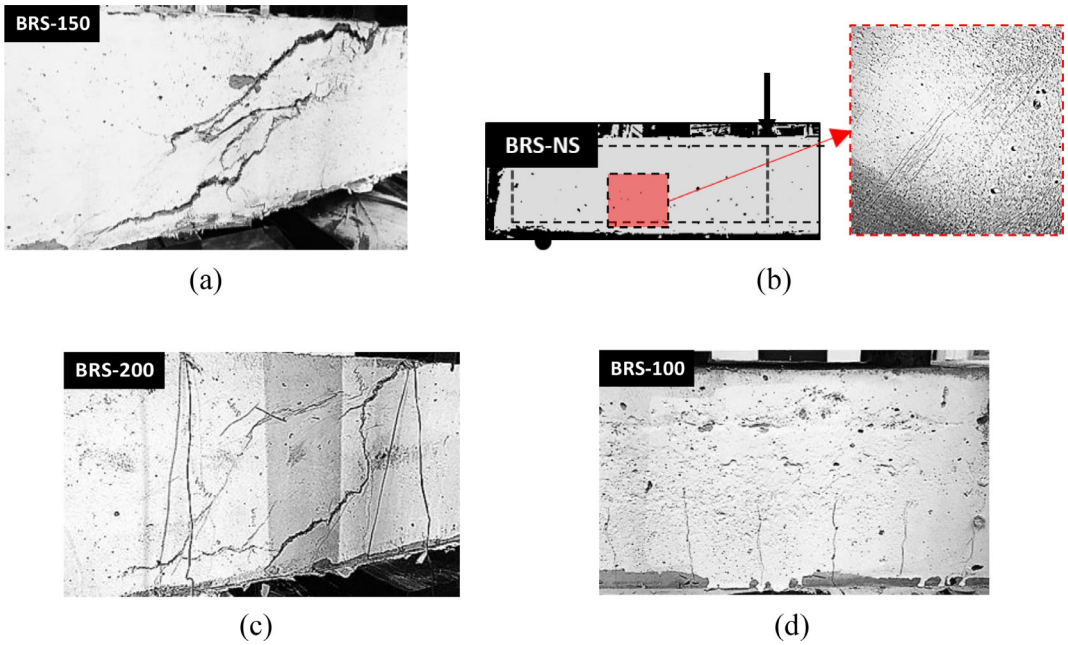

FIGURE 5 Crack pattern of (a) BRS-150 under ultimate failure; (b) BRS-NS under a load of 65 kN; (c) BRS-200 under a load of 320 kN; (d) BRS-100 under a load of 90 kN

3.1.3 | Specimens with different shear spans

Figure 4c shows the load–deflection curves for the beams with different shear span to depth ratios. Due to a lower shear span to depth ratio, the stiffness of beam BRS-S200 was enhanced remarkably compared with BRS-200, resulting in delayed formation of initial cracks. During external loading, a set of inclined struts was formed with multiple diagonal cracks extending from loading point toward the support substantially. When the mid-span deflection reached 18.0 mm, the peak load of 366.6 kN was achieved due to the crushing of SHCC struts, which exhibited the maximum load carrying capacity among all the tested beams. When referring to the specimen BRS-L200 longest shear span, more flexure-shear cracks could be found along the shear span. After reaching its shear strength, the applied load dropped a little and then kept almost constant with increasing the deformation, exhibiting a load––deformation plateau before ultimate failure.

3.2 | Strain analysis of transverse reinforcement

Shear transfer through transverse reinforcement is known as the most important factor for improving the shear carrying capacity of RC and R/SHCC beams. The reinforcement configuration for all tested beams is outlined with dotted lines in Figure 4, and the strain development of selected stirrups is exhibited in Figure 6. Due to damage of strain gauges during beam casting or loading, not all strain data were well collected, therefore, only some specific gauges are selected to exhibit their strain variation, which were marked as red points in Figure 4.

For BFRP-RC beam BRC-150, strain of the selected stirrup did not exhibit any obvious change until the external load reached around 90 kN, as shown in Figure 6a, revealing that all the shear load was only taken by concrete. However, different from concrete, the stirrups in SHCC beam BRS-150 could take the shear load simultaneously with the SHCC matrix from the beginning. When load reaching around 300 kN, a sharp increase of stirrup strain was observed from 2180 to 2650 με, which indicated the yielding of shear reinforcement. After that, the stirrup strain kept almost constant with deflection increasing, during which the deformation was concentrated in SHCC matrix in shear compression zone.

Figure 6b shows the stirrup strain development in specimens with various stirrup ratios. With a stirrup ratio of only 0.24%, the specimen BRS-200 exhibited the most rapid development in the stirrup strain. When the load reached around 280 kN, the yielding of stirrups occurred, and the further increase in shear resistance is solely contributed by the SHCC matrix. When reaching the peak load, the strain of the shear reinforcement did not increase anymore but kept almost constant. After a small postpeak reduction, the shear resistance from SHCC matrix stabilized and entered a long yield plateau at a

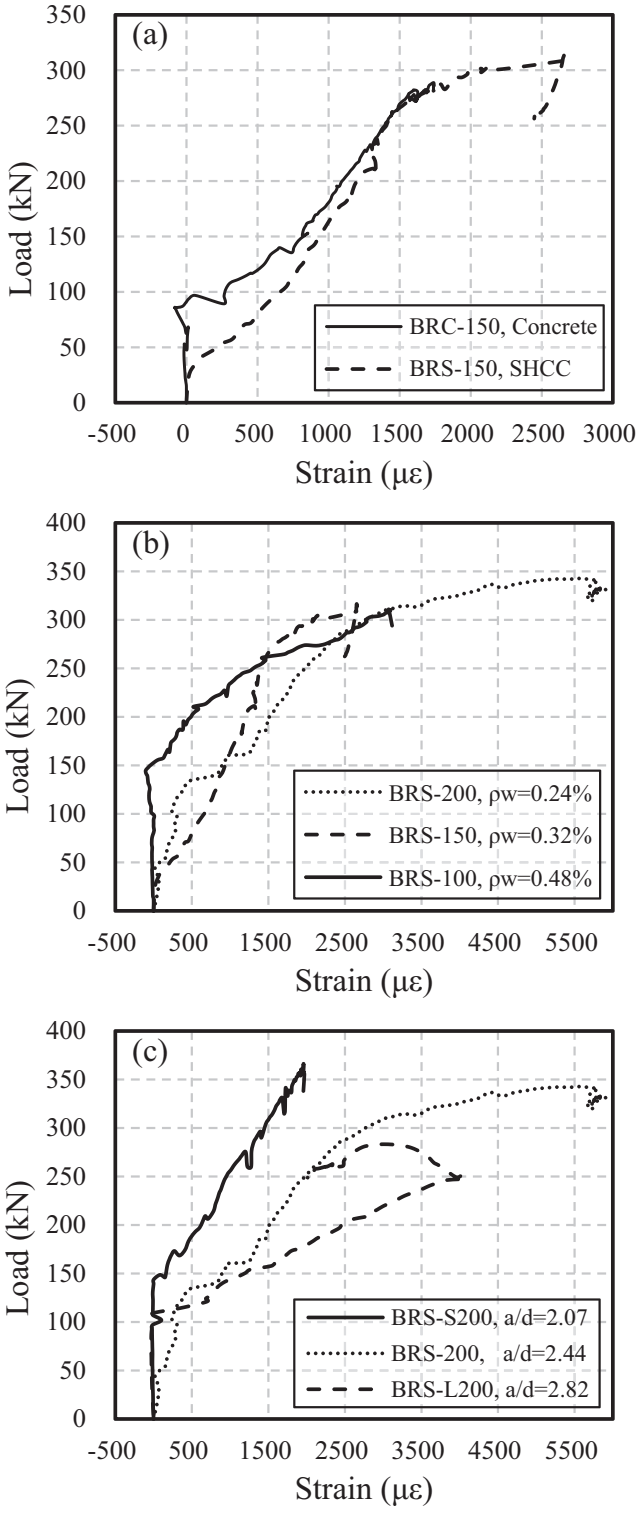

FIGURE 6 Strain variations in selected stirrups: (a) for different matrices; (b) for different transverse reinforcement ratios; (c) for different shear span to depth ratios

deflection of about 23 mm, revealing that the good ductility of specimen BRS-200 was attributed to the stable deformation and load-keeping of the SHCC matrix. For the specimen BRS-100 with the highest shear reinforcement ratio but reduced flexural reinforcement, the strain of the stirrup started to increase until the load reached around 140 kN. After that, the stirrup strain increased rapidly until the specimen finally failed. It gave evidence that localization occurred immediately when the shear crack was formed in specimen BRS-100. It was also found that all selected stirrups yielded in SHCC beams with different shear reinforcement ratios, indicating that SHCC beams with smaller stirrup spacing should have a higher shear contribution from transverse reinforcement. However, a contradictory trend was found in their total shear carrying capacity, and some other shear resistance components would also be significant for the overall shear carrying behavior of BFRP-reinforced SHCC beams, which will be discussed further in the proposed analytical model.

Figure 6c compares the stirrup strain development in beams with different shear spans. For specimen BRS-L200 with the highest shear span to depth ratio, the strain of the stirrup started to increase when the applied load reached about 114 kN, indicating no shear crack occurred in this stage. When the shear crack initiated in the shear span, it opened and propagated quickly with a rapid increase of stirrup strain, which resulted in yielding of stirrup at a load of 190 kN. When the load reached around 250 kN at a deflection of 16.7 mm, the stirrup strain experienced a continuous decrease before final failure of the specimen, indicating a debonding between the stirrup and the SHCC matrix. For the specimen BRS-S200, the stirrup started to undertake shear force at a load of 148 kN, which was quite later than the other two counterpart beams. After that, the stirrup strain increased quite slowly, and when the peak load was achieved, final failure of the specimen occurred and the selected stirrup did not yield yet.

3.3 | Ultimate shear strength and ductility evaluation

To compare the ultimate shear strength of different specimens, the nominal shear stress can be calculated as follows:

$$v = \frac{V}{bd}, \tag{1}$$

where V is the shear force at calculated section and bd is the cross section area of beam specimens. It should be noted that the shear force is only half of the applied load, as shown in Figure 3. With this definition, the nominal ultimate shear strength $v_{u,\exp}$ of tested specimens was obtained according to their ultimate shear force $V_{u,\exp}$, as listed in Table 3.

Ductility describes the ability of material, element, or structure to sustain inelastic deformation prior to collapse without significant loss in load resistance. In general, the ductility coefficient μ of RC members is commonly expressed as the ratio of ultimate displacement to displacement at yielding point, as follows:

$$\mu = \frac{\Delta_u}{\Delta_y}, \tag{2}$$

where Δ_u is defined as the displacement at ultimate failure, and Δ_y is the displacement at yielding point of members.

In this study, Equation (2) is utilized to calculate the ductility coefficient of BFRP-RC members, and the yielding state is defined as the point A through which the two shaded parts showed in Figure 7 have equal areas. Based on this definition, such an equivalent yielding point can effectively be used to evaluate the ductility of BFRP-reinforced SHCC or RC beams.

Table 3 summarizes of the calculated equivalent yielding deflection Δ_y, the deflection at ultimate failure Δ_u, and the ductility index μ for all specimens. The total energy terms E obtained from the areas under the load deflection curves before ultimate failure are also provided. Compared with specimen BRC-150, the ultimate shear strength $v_{u,\exp}$ and ultimate deformation Δ_u of BRS-150 were increased by about 10% and 50% through the utilization of SHCC material. Besides this, a significant increase of 54% in the energy dissipation was found for BRS-150, resulting from a high inelastic energy dissipation based on the unique multiple cracking behavior of SHCC matrix. Among the SHCC specimens, it was found that the ultimate shear strength $v_{u,\exp}$ and ductility of beam BRS-200, which had a transverse reinforcement ratio of 0.24%, was about 1.4 and 1.28 times of those of beam BRS-NS, respectively. It indicated that small shear reinforcement ratio is helpful to increase the shear carrying and deformation capacity of BFRP-reinforced SHCC beams. In addition, since the existence of stirrups can prevent a premature shear failure, the deflection of BRS-200 at ultimate failure was 78.3% larger than that of BRS-NS, resulting in an increase of 180% in energy dissipation compared with specimen BRS-NS. Nevertheless, with increasing the stirrup ratio beyond 0.24%, a degradation of ultimate shear strength and ductility was found, presenting an absonant effect between SHCC matrix and stirrups, which has been mentioned earlier. For SHCC beams of different shear spans, the short-beam BRS-S200 exhibited the maximum load carrying capacity among all the tested beams. However, it showed relatively small ductility due to an abrupt failure with a limited deformation, which should be avoided in member design.

4 | SIMPLIFIED TRUSS–STRUT MODEL FOR PREDICTING SHEAR CARRYING CAPACITY OF R/SHCC BEAMS

There are two basic load resistance mechanisms in RC members subjected to a combination of flexure and shear: truss action and strut action (also called arch action).[37] As shown in Figure 8, in truss action, the reinforcement in compression and tension acts as the top and

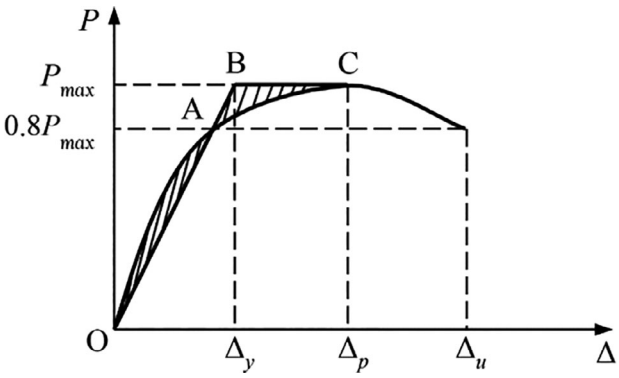

FIGURE 7 Ductility index definition

TABLE 3 Experimental results of test beams

Specimen	$V_{u,\exp}$ (kN)	$v_{u,\exp}$ (MPa)	Δ_y (mm)	Δ_u (mm)	E (kN·m)	μ	Failure mode
BRC-150	144.4	2.29	13.2	24.0	5.00	1.82	Shear-compression
BRS-NS	120.3	1.91	11.2	16.1	2.52	1.43	Shear-tension
BRS-200	171.4	2.72	15.7	28.7	7.06	1.83	Shear-tension
BRS-150	158.2	2.51	17.1	34.0	7.72	1.99	Shear-compression
BRS-100	155.5	2.47	23.6	34.1	6.93	1.45	Shear-compression
BRS-S200	183.1	2.91	12.3	18.8	4.62	1.53	Diagonal-compression
BRS-L200	141.7	2.25	15.7	28.1	5.56	1.79	Shear-tension

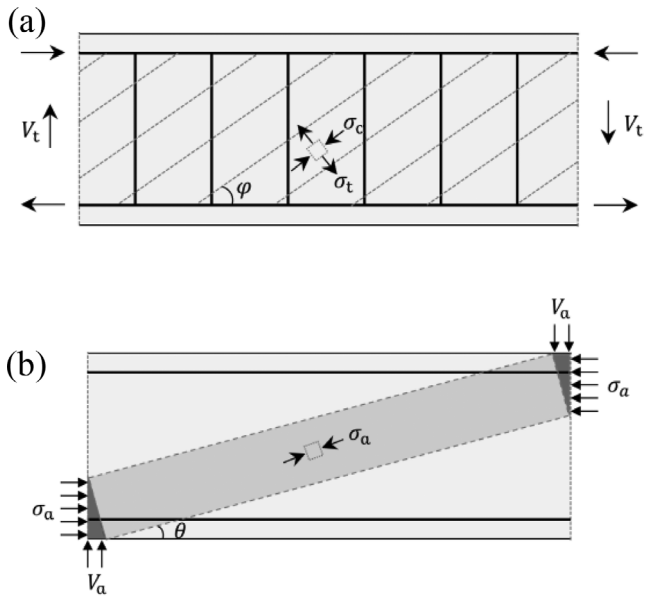

FIGURE 8 Two basic load transfer mechanism: (a) truss action; (b) strut action or arch action

bottom chords separately, the stirrups act as transverse ties, and the web concrete is discretized as a set of parallel compressive struts with a characteristic inclined angle φ, coinciding with the direction of principle compressive stress. The shear in truss action is taken by the transverse reinforcement as well as residual tensile stress perpendicular to concrete struts, which can be represented by V_s and V_t separately. Besides truss action, for beams with low shear span-to-depth ratio, the load could also transfer directly from the loading points to supports, labeled with angle θ, which is named strut action here. In most situations, these two actions exist simultaneously in terms of shear transferring of RC members.

4.1 | Basic assumptions

In this section, the truss–strut model will be adopted for analyzing the shear transfer mechanism for reinforced SHCC beams. Some basic assumptions are adopted to simplify such analysis, as follows:

a. The inclination of compressive web struts should not be the same at different sections and heights due to combination of variable moment and shear force. However, here we assume the inclination of these web struts keeps constant at all sections and heights, with a characteristic inclined angle φ.
b. The effective compressive strength of inclined SHCC struts should be reduced due to multiaxial stress conditions (existence of tensile stress in crossing stirrups) and shear cracks. Due to lack of study on such reduction effect for SHCC, the strength reduction factor for ordinary concrete proposed by EN code is also adopted here for SHCC material,[38] which needs more study in the future:

$$\mu_c = 0.6\left(1 - \frac{f_c}{250}\right), \tag{3}$$

where μ_c is the compressive strength reduction factor, f_c is the compressive strength of SHCC (f_c in MPa).
c. According to the test result as well as some other experimental observations, the crack width of SHCC matrix at peak shear load is ranging from 0.12 to 0.18 mm, which means tension softening has already been reached.[28] Therefore, only reduced residual tensile strength could be taken into consideration for truss action. A reduction factor of tensile strength for SHCC matrix is introduced here:

$$f_{tr} = \mu_t f_t, \tag{4}$$

where f_{tr} is the residual tensile strength and μ_t is the reduction factor.
d. Hydrostatic nodes are assumed for strut action, which means stresses on all faces of triangle strut nodes are equal.

4.1.1 | Truss action

In truss action, the shear force is assumed to be carried by yielding stress along stirrups and residual tensile stress of SHCC perpendicular to inclined struts, as shown in Figure 9. According to the equilibrium of free body shown in Figure 9a,b, we can get the following equations:

$$V_s = bj_t\rho_w\sigma_{wy}\cot\varphi \tag{5a}$$

$$V_t = bj_t\mu_t f_t\cot\varphi \tag{5b}$$

$$V_{truss} = V_s + V_t, \tag{5c}$$

where V_s, V_t, and V_{truss} stand for the shear force undertaken by stirrups, residual tensile stress of SHCC and a summation of them separately. Other symbols can be referred in the Notations.

For beams with low shear span to depth ratio or reinforced with quite dense stirrups, the stirrups could not yield, which means calculating shear component from stirrups with Equation (5a) would overestimate its real shear contribution. To prevent this, an examination

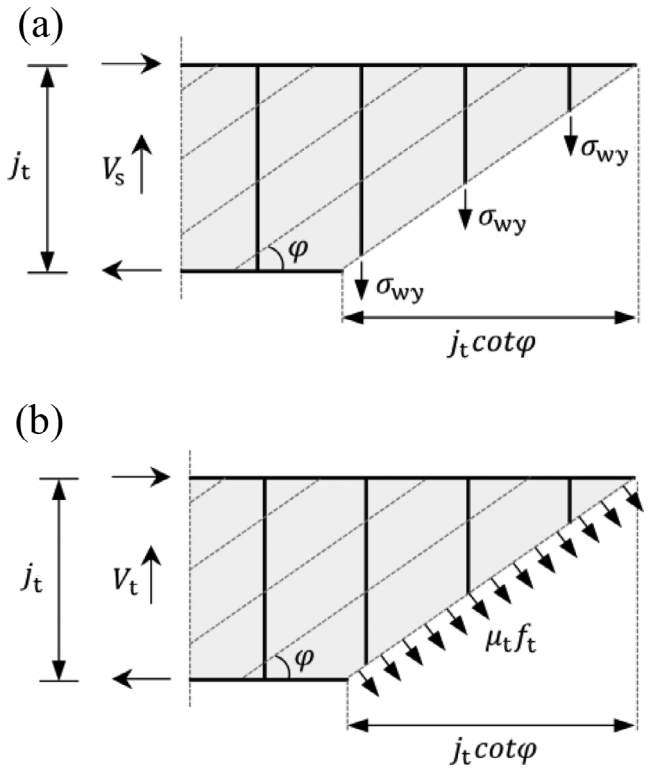

FIGURE 9 Two shear components in truss action: (a) transverse reinforcement; (b) residual tensile stress of SHCC matrix

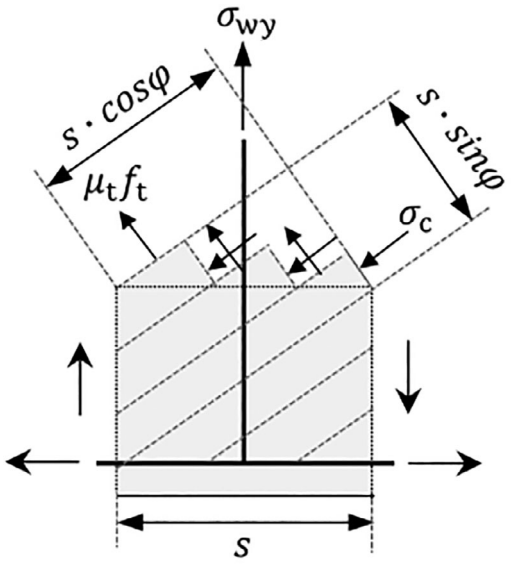

FIGURE 10 Free body equilibrium of stirrup and inclined SHCC struts. SHCC, strain-hardening cementitious composite

of the stress state for inclined SHCC struts is necessary. Based on the free body equilibrium as shown in Figure 10, we can derivate:

$$\sigma_c = \rho_w \sigma_{wy}\left(1+\cot^2\varphi\right)+\mu_t f_t \cot^2\varphi, \tag{6a}$$

where σ_c is the compressive stress of SHCC inclined strut. It could not exceed the compressive strength of crack SHCC, so we have following limiting condition:

$$\sigma_c \le \mu_c f_c, \tag{6b}$$

when substituting σ_c with Equation (6a), we would have:

$$\rho_w \sigma_{wy} \le \frac{\mu_c f_c - \mu_t f_t \cot^2\varphi}{1+\cot^2\varphi}. \tag{6c}$$

If this limiting condition could not be met, then the ultimate failure would happen due to crushing of inclined SHCC struts prior to the yielding of stirrups, the so-called diagonal compression would take place. In such situation, the shear carrying capacity could be determined by the following equation:

$$V_u = \frac{\cot\varphi}{1+\cot^2\varphi} b j_t (\mu_c f_c + \mu_t f_t). \tag{6d}$$

4.1.2 | Strut action

If stirrups yield in truss action and the compressive stress of SHCC strut has not reached its ultimate strength, the SHCC web could continue to undertake the further increase of shear force, during which the strut action comes into play. Here by ignoring the difference in inclination of struts between truss and strut action ($\theta \approx \varphi$), we get:

$$\sigma_c + \sigma_a = \mu_c f_c, \tag{7a}$$

$$\beta = \frac{\sigma_c}{\mu_c f_c} = \frac{\rho_w \sigma_{wy}(1+\cot^2\varphi)+\mu_t f_t \cot^2\varphi}{\mu_c f_c}, \tag{7b}$$

$$\sigma_a = \mu_c f_c - \sigma_c = (1-\beta)\mu_c f_c, \tag{7c}$$

where σ_a is the compressive stress of inclined SHCC struts induced by strut action, and β is the proportion of shear contribution from truss action.

The strut action transfers shear load through a combination of inclined compressive strut, nodes, and horizontal tensile ties, as shown in Figure 11a. Since hydrostatic nodes are assumed, all faces have equal compressive

stress, and the shear load transferred by strut action should be determined by following equation:

$$V_{\text{strut}} = \sigma_a b x_{\text{plate}}, \tag{8a}$$

where V_{strut} is the shear load undertaken by strut action, and x_{plate} is the length of bearing plate. However, V_{strut} could not always increase with larger bearing area, the bearing length of hydrostatic nodes would be limited by shear span to depth ratio, which could be illustrated by Figure 11b. According to the geometrical limiting condition, we can have following relationship between beam size and actual bearing length[39]:

$$x_0 \le \frac{\sqrt{L^2 + D^2} - L}{2}, \tag{8b}$$

$$x_0 = \min\left(x_{\text{plate}}, \frac{\sqrt{L^2 + D^2} - L}{2}\right), \tag{8c}$$

$$V_{\text{strut}} = \sigma_a b x_0, \tag{8d}$$

where x_0 is the effective bearing length of the hydrostatic nodes.

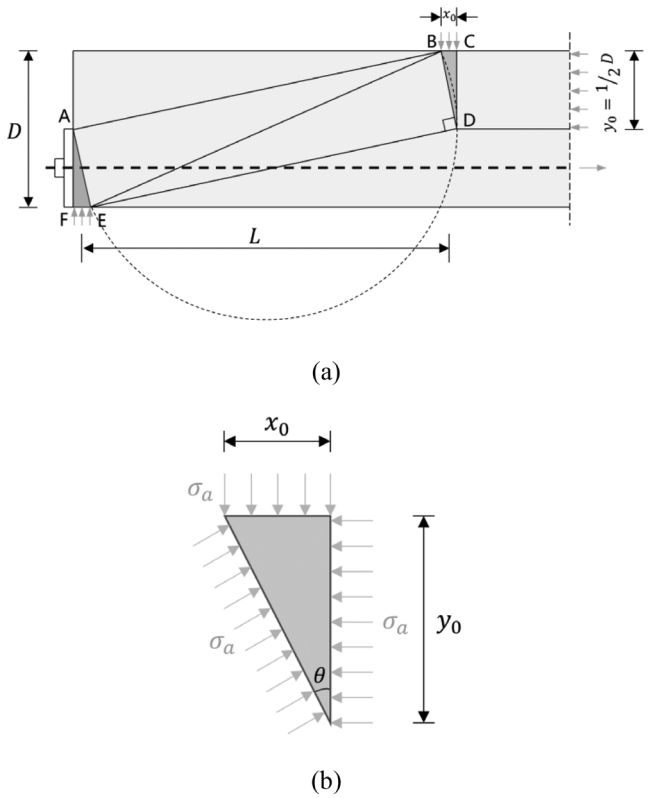

FIGURE 11 Free body equilibrium in inclined SHCC struts: (a) strut action; (b) hydrostatic nodes. SHCC, strain-hardening cementitious composite

4.1.3 | Superposition of two shear transferring actions

Based on preceding derivation, we can now have the total shear carrying capacity of reinforced SHCC beams, as follows:

$$V_{\text{u}} = V_{\text{truss}} + V_{\text{strut}}, \tag{9}$$

where V_{u} is the ultimate shear carrying capacity of reinforced SHCC beams, and Figure 12 exhibits the flow chart for calculating V_{u}.

4.1.4 | Verification of tested R/SHCC beams

To verify the validity of aforementioned truss–strut model for predicting shear carrying capacity of R/SHCC Beams, another 19 SHCC beams reinforced with steel rebars from the literature are also included, for which shear failure was found. All collected beam information is listed in Table 4. There are two important parameters when applying truss and strut model to predict shear strength of reinforced SHCC beams, the reduction factor of tensile strength for SHCC matrix μ_{t} and inclined angle of compressive web struts φ. It should be noted that the inclination φ should be in alignment with the direction of principle compression stress in webs, which is always smaller than the inclination of shear cracks due to shear transfer along cracking surface. However, such difference would be ignored in this analysis and inclination of critical shear crack is just taken as φ, which can be found in Table 4. According to the collected shear strength and crack inclination, we can now calculate the residual tension factor of SHCC μ_t reversely according to the scheme of Figure 12, which is also listed in Table 4.

Figure 13 gives out the relationship between residual tension factor μ_{t} and shear span to depth ratio a/d, longitudinal reinforcement ratio ρ_{l} as well as stirrup ratio ρ_w for both steel-reinforced SHCC beams and BFRP-reinforced ones. It can be found that the residual tension factor μ_{t} decreases with the increase of shear span to depth ratio, no matter for steel or BFRP-reinforced SHCC beams. When comparing steel-reinforced beams with different longitudinal reinforcement ratio, we can find a positive correlation between μ_{t} and ρ_{l}, which means configuring more longitudinal rebars could limit the critical shear crack width and increase residual tensile stress along the truss web. When referring to transverse reinforcement ratio, an obvious negative correlation is found between μ_{t} and ρ_w when shear span to depth ratio is around 3.0; however, when a/d is reduced to around 1.8, residual tension factor μ_{t} keeps almost constant when

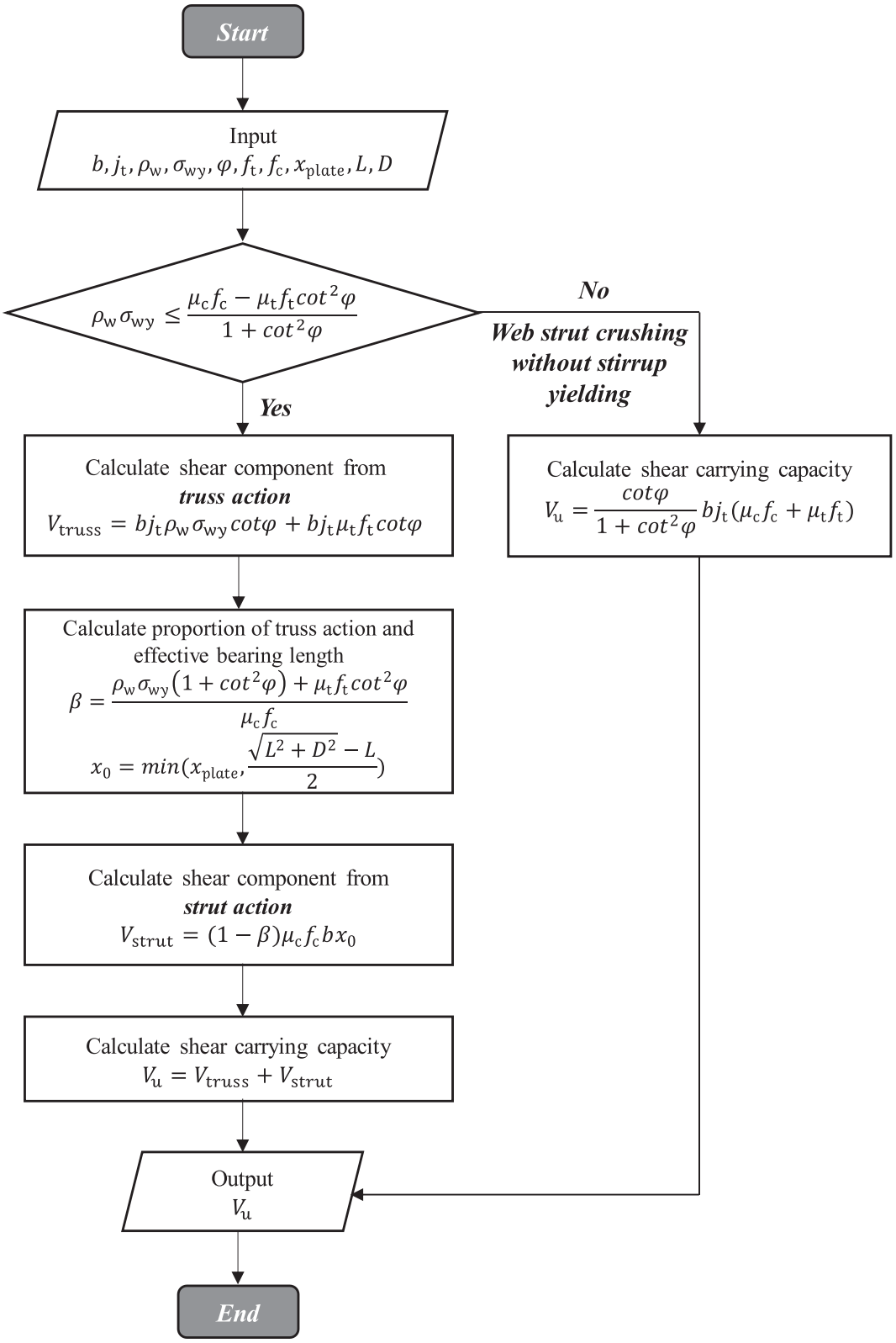

FIGURE 12 Flow chart for calculating shear carrying capacity of R/SHCC beams. SHCC, strain-hardening cementitious composite

stirrup ratio changes. This phenomenon gives evidence that for slender-reinforced SHCC beams with a/d larger than 2.0, the residual tensile stress would be smaller when ultimate shear carrying capacity is reached. On one hand, dense transverse reinforcement could disturb the uniform distribution of fibers; on the other hand, more

TABLE 4 Experimental results of test beams combined with beams found in the literature

Reference	Specimen ID	f_c (MPa)	f_t (MPa)	a (mm)	d (mm)	L (mm)	D (mm)	x_{plate} (mm)	j_t (mm)	ρ_l (%)	ρ_w (%)	σ_{wy} (MPa)	$v_{u,exp}$ (MPa)	μ_t	φ (deg)	$V_{s,pre}$ (kN)	$V_{t,pre}$ (kN)	$V_{strut,pre}$ (kN)	$v_{u,pre}$ (MPa)	$v_{u,pre}/v_{u,exp}$
Shimizu et al.[25] Steel R/SHCC	PVA20-00-L	39.10	4.06	420	233	840	280	-	185	2.54	0.00	0	4.37	0.55	30.0	0.0	105.2	60.8	3.97	0.91
	PVA20-15-L	39.10	4.06	420	233	840	280	-	185	2.54	0.15	295	4.92	0.54	28.0	23.1	105.6	54.4	4.37	0.89
	PVA20-30-L	39.10	4.06	420	233	840	280	-	185	2.54	0.30	295	4.98	0.54	32.0	46.3	106.0	47.9	4.79	0.96
	PVA20-60-L	45.80	4.06	420	233	840	280	-	185	2.54	0.60	334	7.41	0.74	30.0	105.8	106.9	42.2	6.09	0.82
	PVA20-89-L	45.80	4.06	420	233	840	280	-	185	2.54	0.89	334	8.15	0.68	30.0	158.2	107.8	27.4	7.01	0.86
	PVA20-89-S	44.30	4.06	350	233	700	280	-	185	2.54	0.89	427	8.04	0.57	32.0	234.5	189.9	−26.9	9.48	1.18
Hou et al.[26–28] Steel R/SHCC	D-U2	46.22	4.20	300	147	300	180	80	144	2.28	0.00	0	4.82	0.25	38.6	0.0	45.3	54.7	5.67	1.17
	D-U3	46.22	4.20	450	147	450	180	80	144	2.28	0.00	0	3.31	0.10	23.1	0.0	23.5	40.9	3.65	1.10
	D-U4	46.59	4.20	600	147	600	180	80	144	2.28	0.00	0	2.48	0.05	18.6	0.0	16.8	31.5	2.74	1.10
	E-U2	46.59	4.20	300	146	300	180	80	144	3.25	0.00	0	5.47	0.34	32.7	0.0	44.7	55.2	5.71	1.04
	E-U3	45.73	4.20	450	146	450	180	80	144	3.25	0.00	0	3.80	0.15	20.6	0.0	23.3	40.6	3.64	0.96
	E-U4	45.73	4.20	600	146	600	180	80	144	3.25	0.00	0	2.89	0.10	20.1	0.0	16.7	31.0	2.72	0.94
	F-U2	47.76	4.20	300	149	300	180	80	144	4.25	0.00	0	5.81	0.42	32.6	0.0	46.4	56.2	5.74	0.99
	F-U3	47.76	4.20	450	149	450	180	80	144	4.25	0.00	0	3.92	0.20	26.4	0.0	24.0	42.1	3.69	0.94
	F-U4	47.76	4.20	600	149	600	180	80	144	4.25	0.00	0	3.51	0.16	18.3	0.0	17.0	32.2	2.75	0.79
	EU-S3	45.73	4.20	450	146	450	180	80	144	3.25	0.25	316	4.03	0.10	34.4	22.5	17.8	37.0	4.41	1.10
	EU-S6	45.73	4.20	450	146	450	180	80	144	3.25	0.37	316	3.86	0.00	36.2	29.7	15.8	36.1	4.66	1.21
	FU-S3	47.76	4.20	450	149	450	180	80	144	4.25	0.25	316	4.38	0.13	29.8	22.5	18.6	38.4	4.45	1.02
	FU-S6	47.76	4.20	450	149	450	180	80	144	4.25	0.37	316	3.98	0.00	33.0	29.8	16.6	37.5	4.70	1.18
Present test BFRP R/SHCC	BRS-ns	25.05	3.14	650	266	650	300	50	231	1.82	0.00	463	2.15	0.14	30.8	0.0	17.2	89.4	1.91	0.89
	BRS-200	25.05	3.14	650	266	650	300	50	231	1.82	0.24	463	3.07	0.13	34.5	72.1	13.5	69.6	2.78	0.91
	BRS-150	25.05	3.14	650	266	650	300	50	231	1.82	0.32	463	2.83	0.00	36.2	88.9	12.5	65.4	2.99	1.05
	BRS-100	25.05	3.14	650	266	650	300	50	231	0.91	0.48	463	2.78	0.00	44.6	114.7	10.7	59.2	3.30	1.19
	BRS-L200	25.05	3.14	750	266	750	300	50	231	1.82	0.24	463	2.54	0.02	34.9	82.3	5.3	58.6	2.62	1.03
	BRS-S200	25.05	3.14	550	266	550	300	50	231	1.82	0.24	463	3.23	0.23	42.1	63.4	41.6	79.3	3.30	1.02

stirrups would allow larger transverse deformation of the web struts, which means wider shear crack would be found when peak load is reached. Therefore, a weakened residual tensile stress could be expected. However, more well-equipped experimental research is needed to detect the deformation and stress transfer in R/SHCC beams to find out the exact mechanism. In this research, the effect from longitudinal and transverse reinforcement ratio is neglected due to a limitation of experimental data, and only shear span to depth ratio is considered to determine the residual tension factor of SHCC μ_t, which can give a relatively accurate prediction. Through nonlinear regression analysis, equation for calculating μ_t is given for both steel-reinforced SHCC beams and BFRP-reinforced ones, as follows:

$$\mu_t = \begin{cases} 1.9\left(\frac{a}{d}\right)^{-2.3}, & \text{steel}-\text{reinforced SHCC beam} \\ 53.9\left(\frac{a}{d}\right)^{-7.5}, & \text{BFRP}-\text{reinforced SHCC beam} \end{cases}, \tag{10}$$

where a/d is the shear span to depth ratio. When calculated μ_t is larger than 1.0, $\mu_t = 1.0$. The coefficient of determination (R^2) for expression of μ_t is 0.80 and 0.60 for steel and BFRP-reinforced SHCC, respectively.

Figure 14 illustrates the relationship between inclination angle of web struts φ and shear span to depth ratio a/d, longitudinal reinforcement ratio ρ_l as well as stirrup ratio ρ_w for both steel-reinforced SHCC beams and BFRP-reinforced ones. We can find that with shear span to depth ratio decreasing or stirrup ratio increasing, the inclination angle φ would increase. However, the influence from longitudinal reinforcement ratio is inconspicuous. An equation for calculating the inclination angle φ is given as follows based on regression analysis:

$$\varphi = \begin{cases} 43.8 - 6.1\left(\frac{a}{d}\right) - 3771.9\rho_w + 2047.5\rho_w\left(\frac{a}{d}\right), & \text{steel}-\text{reinforced SHCC beam} \\ 60.1 - 12.2\left(\frac{a}{d}\right) + 1096.7\rho_w\left(\frac{a}{d}\right), & \text{BFRP}-\text{reinforced SHCC beam} \end{cases}. \tag{11}$$

The coefficient of determination (R^2) for expression of φ is 0.77 and 0.84 for steel- and BFRP-reinforced SHCC, respectively. From Equation (11), it can be found that for BFRP-reinforced SHCC beams, when the shear span to depth ratio a/d is kept constant, the inclination angle of web struts φ would increase when raising the stirrup ratio ρ_w. However, the residual tension factor μ_t keeps almost constant when stirrup ratio changes. Therefore, the shear resistance from fiber bridging V_t would also decrease due to reduced shear cracking surface area when the stirrup ratio ρ_w increases.

With Equations (10) and (11), the shear carrying capacity can be calculated through flow chart in Figure 12. The ratio of predicted ultimate shear strength to experimental value ($v_{u,pre}/v_{u,exp}$) is listed in Table. 4, a mean of 1.01 and the coefficient of variation (CV) of 0.12 for all collected steel-reinforced SHCC beams are found, and the mean of 1.01 and CV of 0.10 is obtained for tested BFRP-reinforced beams particularly, which indicates a good agreement between the predicted shear resistance and the experimental one for all tested reinforced SHCC beams. Apart from this work, Hou[28] and Shimizu[25] have also proposed two different shear design equations for steel-reinforced SHCC beams, the comparison between experimental and predicted results are also exhibited in Figure 15 and Table 4. For steel-reinforced SHCC beams, both satisfactory performances can be found in proposed truss–strut model and Hou's empirical equation. However, for BFRP-reinforced ones, Hou's equation would always overestimate their shear resistance, this may result from the comparative low elastic modulus of FRP bars compared with that of steel, which could reduce the flexure–shear crack control and shear carrying capacity for reinforced beams.[3,4] The prediction method proposed by Shimizu is also based on truss and strut model.[24,25] However, a constant reduction factor of tensile strength μ_t and inclined angle of compressive web struts φ are assumed in his derivation, the coupling effect between different shear parameters are neglected, and judgment conditions for whether stirrups could reach yield stress are not well adopted, which could cause dangerous overestimation in shear design of R/SHCC beams, as shown in Figure 15c).

5 | DISCUSSION

It has been mentioned that a contradictory trend was found in total shear carrying capacity when configuring more stirrups in BFRP reinforced beams. When comparing specimen BRS-150 with BRS-200, which have the same flexural reinforcement configuration and geometric size but different stirrup ratio, it was interesting to find

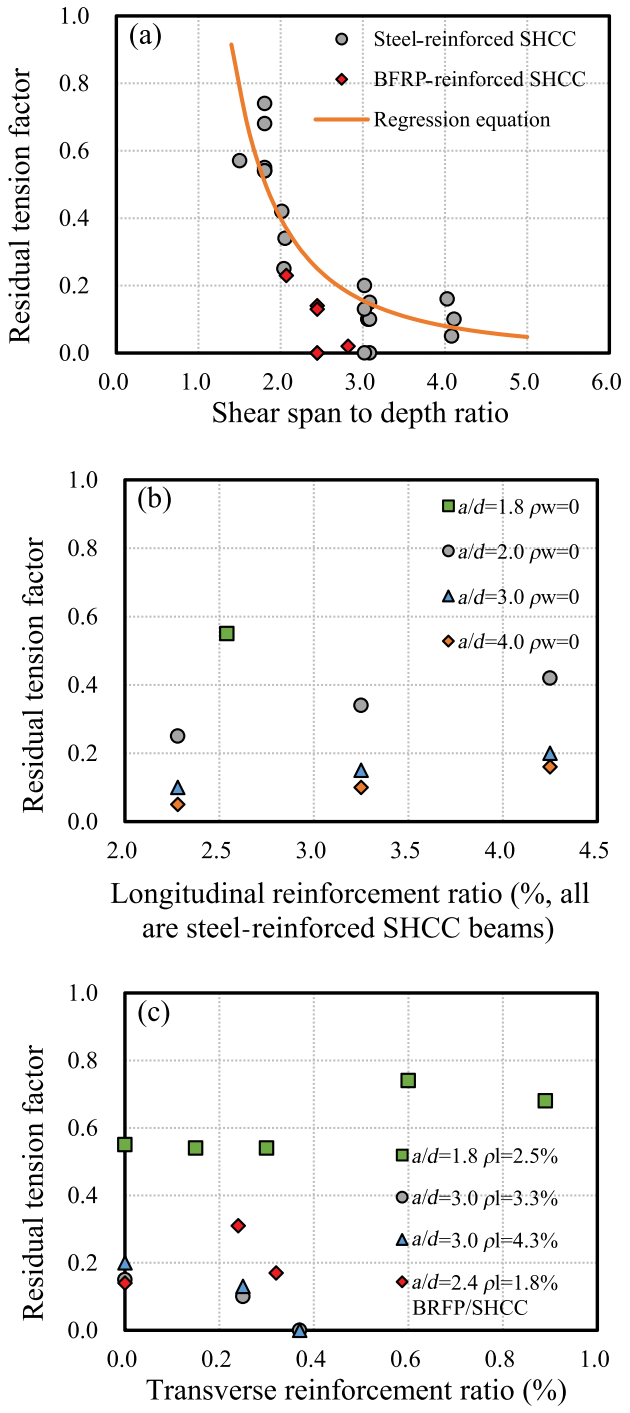

FIGURE 13 Relationship between residual tension factor of SHCC and: (a) shear span to depth ratio; (b) longitudinal reinforcement ratio; (c) transverse reinforcement ratio

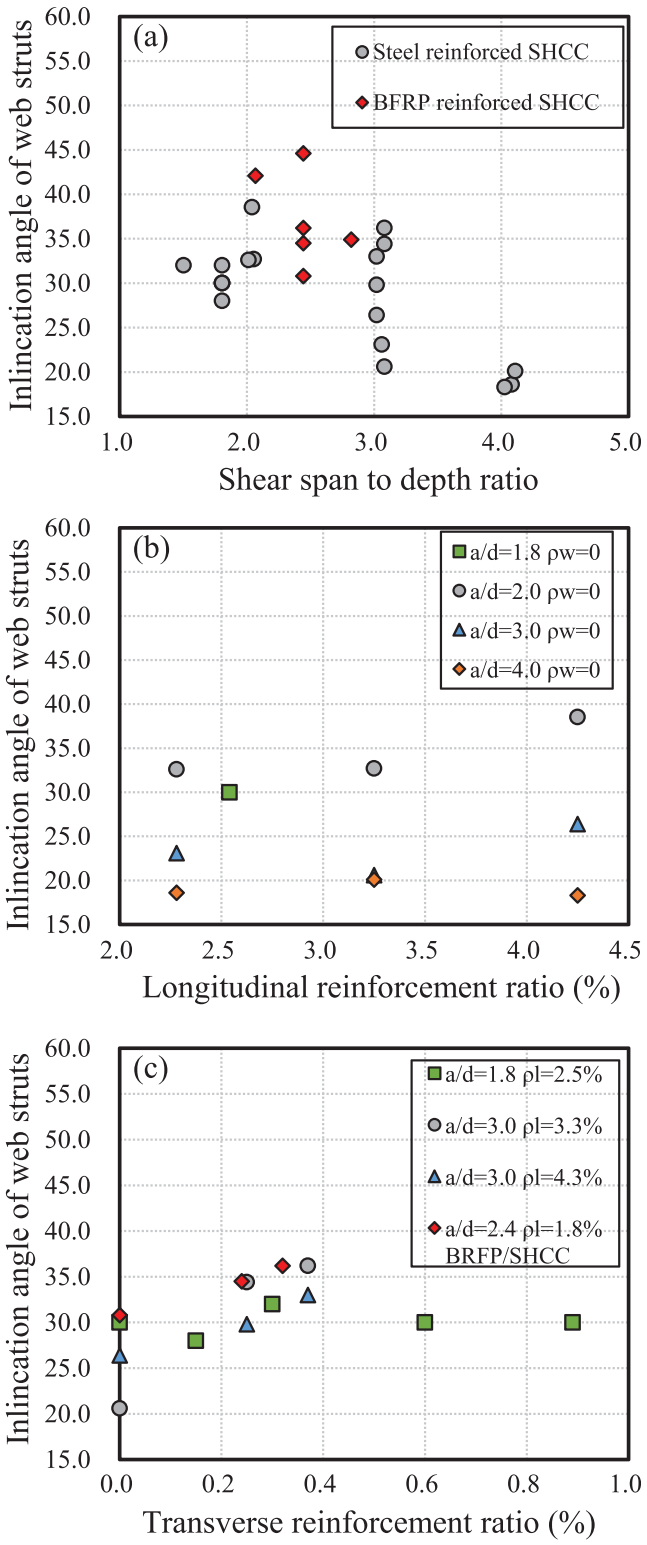

FIGURE 14 Relationship between inclination angle of web struts φ and: (a) shear span to depth ratio; (b) longitudinal reinforcement ratio; (c) transverse reinforcement ratio

that the ultimate shear strength of beam specimen was decreased when more stirrups were provided, which was quite different from the conventional RC beams. A similar phenomenon was also observed by Shimizu et al.[24] and Hou et al.[28] in their experimental work on shear behavior of steel-reinforced SHCC beams. In Shimizu's research, when increasing the stirrup ratio from 0.15% to 0.30%, the ultimate shear strength of reinforced SHCC beams was enhanced only by about 1.4%. In Hou's work, steel-reinforced SHCC beam with 0.25% web

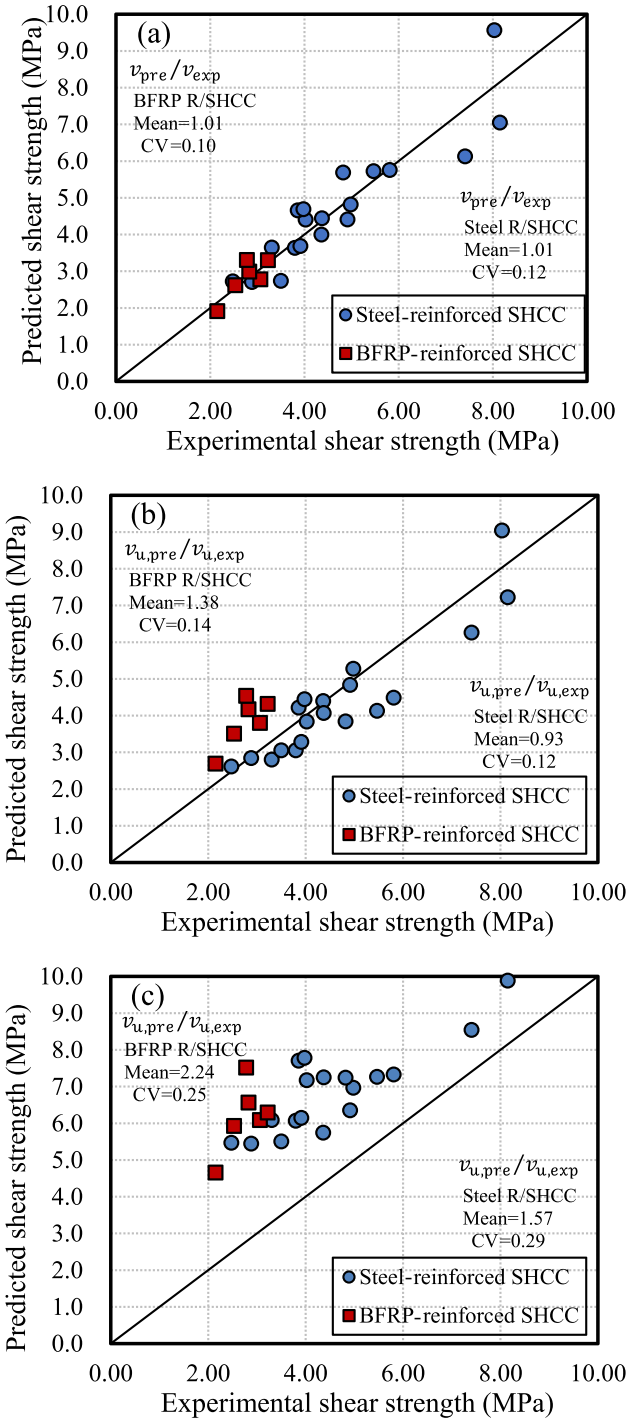

FIGURE 15 Comparison between experimental ultimate shear strength and the predicted value based on: (a) truss-strut model proposed in this research; (b) predicting equation by Hou[28]; (c) predicting equation by Shimizu[25]

reinforcement ratio had higher shear resistance than the counterpart beam with stirrup ratio of 0.37%. It was interpreted by Hou et al. that the shear contribution of SHCC itself reduced with the increase in the transverse reinforcement ratio due to the restriction of stirrups. The increase of shear reinforcement would lead to a redistribution of shear stress and disturb the uniform strain field in SHCC matrix in the shear span. Then the flexure–shear crack could open and propagate quickly upon its existing, which resulted in a premature failure of fiber bridging and localization during the early loading stage. When the peak load was achieved, the crack extended significantly and a narrow shear compression zone was obtained. As a result, the shear contribution of SHCC itself as well as the overall shear carrying capacity of specimens could exhibit a decreasing tendency with the increase in transverse reinforcement ratio within a certain range.

To make the shear transferring mechanism clearer, a parametric analysis is conducted to find the relationship between stirrup ratio and different shear strength components based on the proposed truss and strut model, as shown in Figure 16. The same geometric and material parameters for tested BFRP-reinforced SHCC beams in this research are utilized for the case study. According to Equations (5b) and (11), with stirrup ratio increasing, the inclined angle of compressive struts in truss action would increase, which would result in a reduced shear cracking surface area and shear resistance from fiber bridging, as shown in Figure 16(a). Besides, the proportion of shear contribution from strut action $(1-\beta)$ would also decrease according to Equations (7) and (8), which causes the decrease of shear resistance from strut action, as shown in Figure 16(b). As for the shear contribution from transverse reinforcement, according to Equation (5a), although more stirrups could be provided, the increasing inclination angle φ may cause fewer stirrups being crossed and activated to take the shear load. Figure 16c exhibits the relationship between V_s and ρ_w, it can be found that the shear load undertaken by stirrups would first increase and then decrease when raising stirrup ratio. On the whole, there would be very little enhancement or even degradation in terms of total shear strength when the stirrup ratio reaches around 0.5% for BFRP reinforced SHCC beams, as shown in Figure 16d. Therefore, enhancing shear capacity by increasing stirrup ratio would not be suitable for shear critical SHCC members.

Although the proposed analytical model does not exactly match test results, a consistent tendency is achieved when referring to the relationship between shear carrying capacity and stirrup ratio for R/SHCC beams. Besides, it should be mentioned that the influence of longitudinal reinforcement ratio ρ_l is not considered in shear equation of this research. It is found that higher ρ_l could increase the reduction factor of tensile strength μ_t for R/SHCC beams without stirrups. However, the effect of longitudinal reinforcement ratio on shear resistance for R/SHCC beams with stirrups is still unknown due to lack of experimental results. More precise equation for

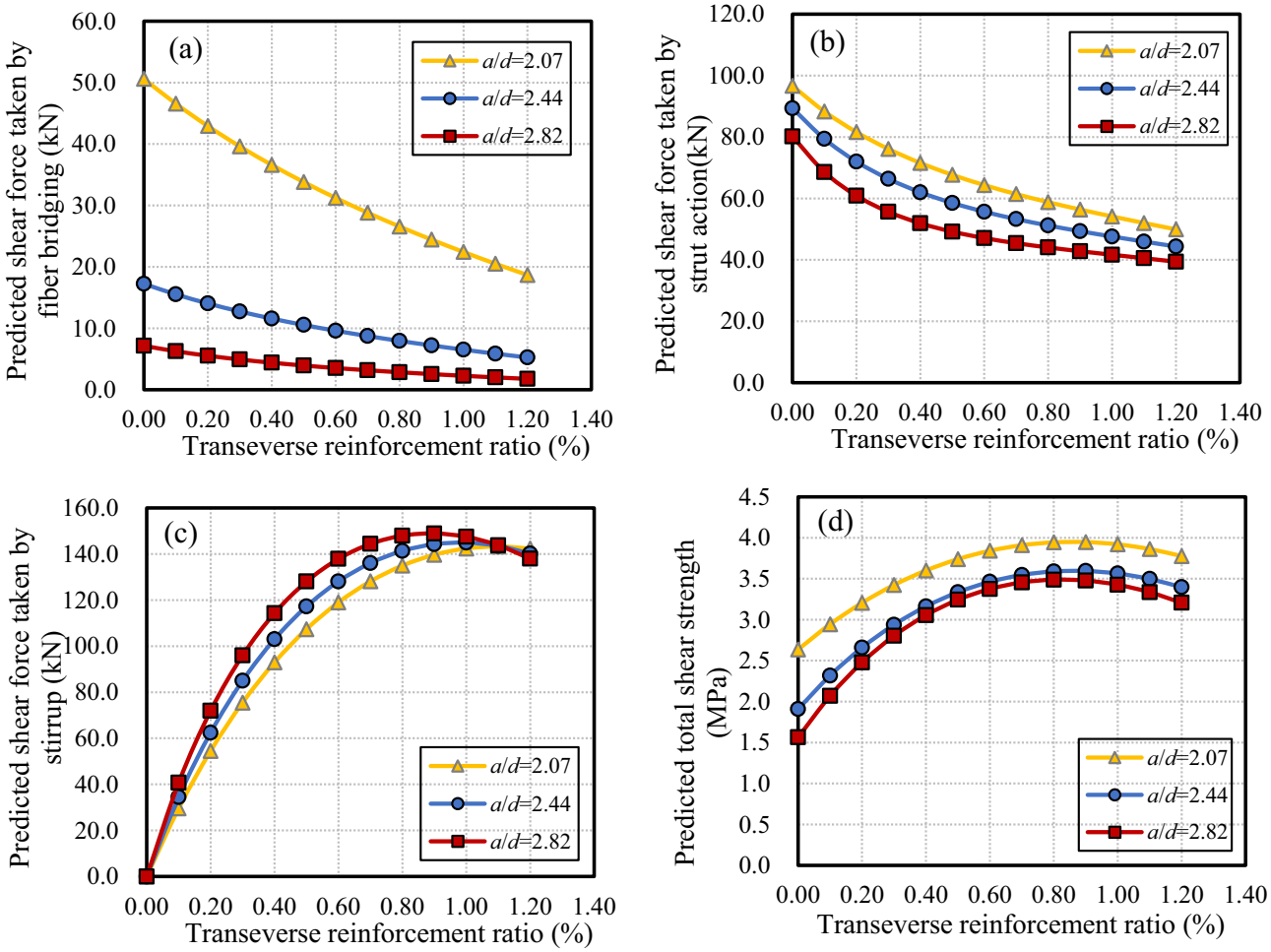

FIGURE 16 Relationship between stirrup ratio and different shear strength components predicted by proposed truss–strut model: (a) shear force undertaken by fiber bridging; (b) shear force undertaken by strut action; (c) shear force undertaken by stirrup; (d) total shear strength

calculating μ_t and φ could be proposed based on the preceding simplified truss–strut model when more test results are acquired. Furthermore, the size effect is also considered to be negligible. Size effect has been proved as an essential parameter for shear design of RC beams, which has been incorporated into some RC design codes for more than 2 dozen years ago.[40–42] Previous studies have shown that beam with larger scale would store higher strain energy.[43] When a critical shear crack is created, the residual tensile stresses across crack come into resisting the energy release. Different from brittle concrete, for large-scale R/SHCC members, the energetic size effect due to unsteady localization of cracks would be eliminated because of the inherent strain hardening behavior and outstanding cracking control capacity of SHCC material.[44] For reinforced FRC beam with strain-softening behavior, size effect has been found greatly weakened or even eliminated due to an enhanced crack control according to previous experimental results.[45] Nevertheless, further experimental research on size effect should be carried out for shear of R/SHCC members.

6 | CONCLUSION

In this paper, a number of FRP-reinforced beams with different reinforcement configurations, effective shear span to depth ratios and matrix types (SHCC and conventional concrete) have been tested to study their shear behaviors under four-point bending. The experimental results were presented mainly concerning the failure mode, crack propagation, load–deflection behavior, shear cracking strength, ultimate shear strength and ductility of specimens. Besides this, the prediction equation based on strut and tie model is proposed in this research. The model is verified based on presented experimental study and literature data for steel-reinforced SHCC, and parametric analysis is conducted to evaluate their various shear transferring components. The following conclusions are drawn from this work:

- The substitution of conventional concrete with SHCC can improve the shear properties in terms of deformation capacity and energy dissipation for

BFRP-reinforced beams, and slightly in terms of strength.

- The ductility and deformation capacity of specimens under shear are dominated by the matrix in shear compression zone. Because the compressive strain at the ultimate strength of SHCC is nearly twice that of conventional concrete, the stirrup could deform continuously until yielding without crushing of SHCC matrix in the shear compression zone.
- Limited amount of shear reinforcement can control the propagation of inclined cracks efficiently, ensuring the integrity of SHCC in shear compression zone and effective fiber bridging across cracks and achieve full shear resistance from both shear stirrups and SHCC matrix. Although reinforced with fewer stirrups, the FRP-reinforced SHCC beam exhibits much higher shear carrying capacity and deformation ability compared both with the concrete and SHCC beam with more dense stirrups, which suggests that decreasing shear reinforcement is feasible when the concrete matrix is replaced by SHCC.
- Enhancing shear capacity by increasing stirrup ratio is not suitable for shear critical SHCC members. The dense configuration of transverse reinforcement will lead to a steeper inclination and premature localization of shear crack, which could reduce the shear resistance from fiber bridging, strut action as well as transverse reinforcement.
- With decreasing shear span to depth ratio, FRP-reinforced SHCC beam exhibits significantly enhanced stiffness and load carrying capacity under shear; however, the ductility becomes much smaller since a brittle diagonal compression failure occurred.
- Based on a simplified truss–strut model, a design scheme for calculating ultimate shear carrying capacity of steel or BFRP bars reinforced SHCC beams are proposed. Parameters include shear span to depth ratio, transverse reinforcement, compressive and tensile strength of SHCC, height of beam section, and length of load-bearing plate. A good agreement has been demonstrated between experimental and prediction results.

NOTATIONS

a	shear span
d	effective depth of beam section
b	width of beam section
L	distance from loading point to support
D	height of beam section
ρ_{l}	longitudinal reinforcement ratio
ρ_{w}	transverse reinforcement ratio
v	nominal shear stress
V	shear force at calculated section
$v_{u,\mathrm{exp}}$	experimental nominal shear stress at ultimate load
$V_{u,\mathrm{exp}}$	experimental shear force at ultimate load
μ	ductility coefficient
Δ_{u}	displacement at ultimate failure
Δ_{y}	displacement at yielding point of members.
V_{s}	shear resistance of transverse reinforcement
V_{t}	shear resistance of residual tensile stress perpendicular to concrete struts
φ	characteristic inclined angle of compressive struts in truss action
μ_{c}	compressive strength reduction factor
f_{c}	compressive strength of SHCC
f_{t}	tensile strength of SHCC
f_{tr}	residual tensile stress
μ_{t}	reduction factor of residual tensile stress for SHCC matrix
j_{t}	distance between top and bottom flexural reinforcement, or $0.8D$
σ_{wy}	yielding stress of transverse reinforcement
σ_{c}	compressive stress of SHCC inclined struts induced by truss action
σ_a	compressive stress of inclined SHCC struts induced by strut action
β	proportion of shear contribution from truss action
V_{strut}	shear load undertaken by strut action
V_{truss}	shear load undertaken by truss action
x_{plate}	length of bearing plate
x_0	effective bearing length of hydrostatic nodes
$v_{\mathrm{u,pre}}$	predicted nominal shear stress at ultimate load
$V_{\mathrm{s,pre}}$	predicated shear force undertaken by transverse reinforcement
$V_{\mathrm{t,pre}}$	predicated shear force undertaken by fiber bridging of SHCC matrix
$V_{\mathrm{strut,pre}}$	predicated shear force undertaken by strut action

ACKNOWLEDGMENT

The work is financially supported by the National Natural Science Foundation of China (No. 51778131).

DATA AVAILABILITY STATEMENT

Research data are not shared.

ORCID

Mladena Luković https://orcid.org/0000-0002-9254-6937

REFERENCES

1. Ghazizadeh S, Cruz-Noguez CA, Talaei F. Analytical model for hybrid FRP-steel reinforced shear walls. Eng Struct. 2018;156:556–66.
2. Cai ZK, Wang DY, Wang ZY. Full-scale seismic testing of concrete building columns reinforced with both steel and CFRP bars. Compos Struct. 2017;178:195–209.
3. El-Nemr A, Ahmed EA, Benmokrane B. Flexural behavior and serviceability of normal and high strength concrete beams reinforced with glass fiber-reinforced polymer bars. ACI Struct J. 2013;110:1077–88.
4. Pecce M, Manfredi G, Cosenza E. Experimental response and code models of GFRP RC beams in bending. J Compos Constr. 2000;4:182–90.
5. Sonobe Y, Fukuyama H, Okamoto T, Kani N, Kimura K, Kobayashi K, et al. Design guidelines of FRP reinforced concrete building structures. J Compos Constr. 1997;1:90–115.
6. Thériault M, Benmokrane B. Effects of FRP reinforcement ratio and concrete strength on flexural behavior of concrete beams. J Compos Constr. 1998;2:7–16.
7. Tureyen AK, Frosch RJ. Shear tests of FRP-reinforced concrete beams without stirrups. ACI Struct J. 2002;99:427–34.
8. El-Sayed AK, El-Salakawy EF, Benmokrane B. Shear strength of FRP-reinforced concrete beams without transverse reinforcement. ACI Struct J. 2006;103:235–43.
9. Li VC, Wang S. Flexural behaviors of glass fiber-reinforced polymer (GFRP) reinforced engineered cementitious composite beams. ACI Mater J. 2002;99:11–21.
10. Yuan F, Pan J, Leung CKY. Flexural behaviors of ECC and concrete/ECC composite beams reinforced with basalt fiber-reinforced polymer. J Compos Constr. 2013;17:591–602.
11. Li VC. On engineered cementitious composites (ECC): a review of the material and its applications. J Adv Concrete Technol. 2003;1:215–30.
12. Hou L, Xu R, Chen D, Xu S, Aslani F. Seismic behavior of reinforced engineered cementitious composite members and reinforced concrete/engineered cementitious composite members: a review. Struct Concr. 2020;21:199–219.
13. Fischer G, Li VC. Deformation behavior of fiber-reinforced polymer reinforced engineered cementitious composite (ECC) flexural, members under reversed cyclic loading conditions. ACI Struct J. 2003;100:25–35.
14. Hossain KMA. Bond strength of GFRP bars embedded in engineered cementitious composite using RILEM beam testing. Int J Concr Struct M. 2018;12:6.
15. Jin H, Li F, Hu D. Research on the flexural performance of reinforced engineered cementitious composite beams. Struct Concr. 2021;1–23. https://doi.org/10.1002/suco.202100012
16. Xu L, Pan J, Lu C, Yin W. Development mechanism of plastic hinge in reinforced engineered cementitious composite beams under monotonic loading. Struct Concr. 2019;20:252–66.
17. Kanakubo T, Shimizu K, Nagai S, Kanda T. Shear transmission on crack surface of ECC. 7th International Conference on Fracture Mechanics of Concrete and Concrete Structures. Jeju, Republic of Korea: International Association of Fracture Mechanics for Concrete and Concrete Structures; 2010. p. 1623–1630.
18. Paegle I, Fischer G. Phenomenological interpretation of the shear behavior of reinforced engineered cementitious composite beams. Cement Concr Compos. 2016;73:213–25.
19. Wu C, Leung CKY, Li VC. Derivation of crack bridging stresses in engineered cementitious composites under combined opening and shear displacements. Cement Concr Res. 2018;107:253–63.
20. Li VC, Mishra DK, Naaman AE, Wight JK, Lafave JM, Wu H, et al. On the shear behavior of engineered cementitious composites. Adv Cem Bas Mat. 1994;1:142–9.
21. van Zijl GPAG. Improved mechanical performance: shear behaviour of strain-hardening cement-based composites (SHCC). Cement Concr Res. 2007;37:1241–7.
22. Kang S, Tan K, Zhou X, Yang B. Experimental investigation on shear strength of engineered cementitious composites. Eng Struct. 2017;143:141–51.
23. Kanda T, Lin Z, Li VC. Application of pseudo strain-hardening cementitious composites to shear resistant structural elements. 3th International Conference on Fracture Mechanics of Concrete and Concrete Structures. Gifu, Japan: International Association of Fracture Mechanics for Concrete and Concrete Structures; 1998.p. 1477–90.
24. Shimizu K, Kanakubo T, Kanda T, Nagai S. Shear behavior of steel reinforced PVA-ECC beams. 13th World Conference on Earthquake Engineering. Vancouver, BC, Canada: World Conference on Earthquake Engineering; 2004.
25. Kanakubo T, Shimizu K, Kanda T, Nagai S. Evaluation of bending and shear capacities of HPFRCC members toward the structural application. Proceedings of the Hokkaido University COE Workshop on High Performance Fiber Reinforced Composites for Sustainable Infrastructure System. Sapporo, Japan: Hokkaido University; 2007.p. 1–10.
26. Xu S, Hou L, Zhang X. Flexural and shear behaviors of reinforced ultrahigh toughness cementitious composite beams without web reinforcement under concentrated load. Eng Struct. 2012;39:176–86.
27. Xu S, Hou L, Zhang X. Shear behavior of reinforced ultrahigh toughness cementitious composite beams without transverse reinforcement. J Mater Civil Eng. 2012;24:1283–94.
28. Hou L, Xu S, Zhang X, Chen D. Shear behaviors of reinforced ultrahigh toughness cementitious composite slender beams with stirrups. J Mater Civil Eng. 2014;26:466–75.
29. Zhang Y, Deng M. Shear tests of engineered cementitious composites: mechanical behavior and toughness evaluation. Struct Concr. 2021;22:2482–92.
30. Wu C, Pan Z, Mo YL, Li M, Meng S. Modeling of shear-critical reinforced engineered cementitious composites members under reversed cyclic loading. Struct Concr. 2018;19:1689–701.
31. Ministry of Housing and Urban-Rural Development of the People's Republic of China. Code for design of concrete structure (GB50010-2010). Beijing, China: China Standard Press; 2010.
32. Shehata E, Morphy R, Rizkalla S. Fibre reinforced polymer shear reinforcement for concrete members: behaviour and design guidelines. Can J Civil Eng. 2000;27:859–72.
33. Lee C, Ko M, Lee Y. Bend strength of complete closed-type carbon fiber-reinforced polymer stirrups with rectangular section. J Compos Constr. 2014;18:04013022.
34. Issa MA, Ovitigala T, Ibrahim M. Shear behavior of basalt fiber reinforced concrete beams with and without basalt FRP stirrups. J Compos Constr. 2016;20:04015083.
35. CSA. Design and construction of building structures with fibre-reinforced polymers. Mississauga, ON, Canada: CSA; 2012.

36. ACI Committee. 440. Guide for the design and construction of structural concrete reinforced with FRP bars. Farmington Hills, MI: ACI; 2015.
37. Ichinose T. A shear design equation for ductile R/C members. Earthq Eng Struct D. 1992;21:197–214.
38. European Committee for Standardization (CEN). Eurocode 2: Design of concrete structures—Part 1-1: General rules and rules for buildings. EN 1992-1-1. Brussels, Belgium: European Committee for Standardization (CEN); 2004.
39. Nielsen MP, Linh CH. Limit analysis and concrete plasticity. Boca Raton, FL: CRC Press; 2016.
40. Bažant ZP, Yu Q. Designing against size effect on shear strength of reinforced concrete beams without stirrups: I. Formulation J Struct Eng. 2005;131(12):1877–85.
41. Alam MS, Hussein A. Size effect on shear strength of FRP reinforced concrete beams without stirrups. J Compos Constr. 2013;17(4):507–16.
42. Zararis PD, Papadakis GC. Diagonal shear failure and size effect in RC beams without web reinforcement. J Struct Eng. 2001;127(7):733–42.
43. Bažant ZP, Kim SS. Size effect in shear failure of longitudinally reinforced beams. ACI J. 1984;81(5):456–68.
44. Lepech M, Li VC. Size effect in ECC structural members in flexure. IaFraMCos, Vail Colorado: Fract Mech Concr Struct; 2004.p. 1059–66.
45. Dinh HH, Parr GJ, Wight JK. Shear behavior of steel fiber-reinforced concrete beams without stirrup reinforcement. ACI Struct J. 2010;107(5):597–606.

AUTHOR BIOGRAPHIES

Dawei Gu
School of Civil Engineering
Southeast University
Nanjing, China
dwgu@seu.edu.cn

Jinlong Pan
School of Civil Engineering
Southeast University
Nanjing, China
cejlpan@seu.edu.cn

Mladena Luković
Faculty of Civil Engineering and Geosciences
Delft University of Technology
Delft, The Netherlands
m.lukovic@tudelft.nl

Jixuan He
School of Civil Engineering
Southeast University
Nanjing, China
hejixuan1005@gmail.com

How to cite this article: Gu D, Pan J, Luković M, He J. Experimental and analytical study on shear behavior of strain-hardening cementitious composite beams reinforced with fiber-reinforced polymer bars. Structural Concrete. 2022;1–20. https://doi.org/10.1002/suco.202100544